

# Possible spin liquid states with parton Fermi surfaces in SU(3) ring-exchange model on the triangular lattice

Hsin-Hua Lai

National High Magnetic Field Laboratory, FSU, Tallahassee, Florida 32310, USA

(Dated: October 16, 2012)

We consider a SU(3) ring-exchange model on a triangular lattice. Unlike the SU(2) case, under perturbation expansion of the SU(3) Hubbard model, the three-site ring exchange is present as well as the usual four-site ring exchange. Interestingly, the three-site ring exchange differs from the usual two-site and four-site exchanges by a minus sign and is ferromagnetic. We first present numerical site-factorized state studies on this model which shows three-sublattice order and a ferromagnetic phase. We further study the model using slave-fermion mean field in which we rewrite the exchange operators in terms of three flavors of fermions. We find the main competing trial states are the trimer state (triangular plaquette state) and the gapless U(1) spin liquid states with parton Fermi surfaces which include both the uniform zero-flux spin liquid state, and the uniform  $\pi$ -flux spin liquid state. Furthermore, we find there are possible pairing instabilities of the zero-flux (Fermi surface) spin liquid state toward a  $f$ -wave gapless (nodal) spin liquid state and the  $\pi$ -flux (Fermi surface) spin liquid state toward an interesting exotic  $s$ -wave “gapless” spin liquid state with two flavors of fermions paired up while one flavor of fermions remains gapless.

## I. INTRODUCTION

In recent years, the cold atomic systems have become a powerful tool to realize strongly-correlated systems, including N-flavor Hubbard model on different lattices. Such systems consisting of several flavors of interacting fermions can be realized as different hyperfine states of alkali atoms [1] or nuclear spin states of ytterbium [2–4] or alkaline-earth atoms [5–7]. A model Hamiltonian to describe such systems is the N-flavor fermionic Hubbard model [1, 6, 8]

$$H = -t \sum_{\langle jk \rangle} \sum_{\alpha} \left[ c_j^{\alpha\dagger} c_k^{\alpha} + \text{H.c.} \right] + U \sum_j \sum_{\alpha, \beta} n_j^{\alpha} n_j^{\beta}, \quad (1)$$

where  $\alpha, \beta$  run over the different flavors,  $\langle jk \rangle$  runs over pairs of nearest neighbors on the lattice, and  $j$  runs over all lattice sites.

The most common case is when  $N = 2$ , which corresponds to the usual spin-1/2 Hubbard model. If we focus on the half-filling condition, i.e., when each site is occupied by exactly one fermion, the system undergoes metal-to-Mott insulator phase transition for sufficiently large repulsion  $U$ . In experiments on cold atoms, the transition to a Mott insulator has recently been observed. [9, 10] In the large  $U$  regime, it is generally accepted that the ground state is well-captured by the usual anti-ferromagnetic (AF) Heisenberg model and the charge degrees of freedom are completely frozen out. However, in the regime where  $U$  is not sufficiently large compared with the hopping strength  $t$ , the ground state is not well-understood. It is possible that the strong charge fluctuations play important role for stabilizing “gapless” spin liquid phases in this regime. [11, 12]

For the more general case with  $N > 2$ , [13, 14] if we focus on certain fillings, the Mott insulating states will also emerge. In this case, the spin order is not understood even in the large  $U$  limit in which we can only focus on the Heisenberg-like (two-site exchange) Hamiltonian

$$H_2 = J \sum_{\langle jk \rangle} P_{jk}, \quad (2)$$

where  $P_{jk}$  is so-called two-site exchange operator, which permutes the fermions between two nearest-neighbor sites as  $P_{jk}|\alpha, \beta\rangle = |\beta, \alpha\rangle$ , where the  $\alpha, \beta$  represent the spin states at sites  $j$  and  $k$ . For  $N = 3$ , there has been numerical evidence on such SU(3) Heisenberg model on a triangular lattice suggesting three-sublattice-ordered ground state in this regime. [15]

The situation becomes more complex if  $t/U \sim O(1)$ , since in this regime the two-site exchange Hamiltonian is not sufficient to capture the essential physics and higher ordered contributions such as ring exchanges should be taken into account. In this paper, we focus on this regime and consider the SU(3) ring-exchange model on the triangular lattice. Motivated by the perturbative studies of the SU(3) Hubbard model at 1/3 filling, we include the “ferromagnetic” three-site ring exchanges and the “anti-ferromagnetic” four-site ring exchanges in the model whose Hamiltonian is given in Eq. (3). With the interplay between the ring exchanges, we conjecture that the Quantum spin liquid (QSL) states [16, 17] can arise due to the strong frustration.

In this work, we first study the ordered phases using the site-factorized ansatz. [18] We find that the phase diagram contains the three-sublattice ordered phase, similar to the phase found in Ref. 15, and the ferromagnetic state. We further study this model using slave-fermion trial states. After performing numerical full optimization of the trial energy, we consider the three ansatz states such as the uniform zero-flux and  $\pi$ -flux gapless (Fermi-surface) spin liquid state and the trimer (plaquette) state. Furthermore, we consider several pairing instabilities and find that there is a pairing instability of the zero-flux spin liquid state toward a  $f$ -wave (nodal) spin liquid state; there is a pairing instability of the uniform  $\pi$ -flux spin liquid state toward a interesting exotic  $s$ -wave spin liquid state with two flavors of fermions paired up while one flavor of fermions remains gapless.

The paper is organized as follows. In Sec. II we define explicitly the model Hamiltonian we will study in the paper. In Sec. II A we use the site-factorized ansatz to study the ordered states in this ring-exchange model. In Sec. II B we use the

slave-fermion representation to rephrase the SU(3) Hamiltonian in terms of the three-flavor fermionic Hamiltonian and perform the fermionic mean-field treatment of the model. We further study the possible pairing instability in the spin liquids regime. In Sec. III we conclude with some discussions.

## II. SU(3) MODEL WITH RING EXCHANGE TERMS

The model Hamiltonian we consider is

$$H_{SU(3)} = J \sum_{\text{bonds}} P_{12} - K_3 \sum_{\text{triangles}} [P_{123} + \text{H.c.}] + K_4 \sum_{\text{rhombi}} [P_{1234} + \text{H.c.}], \quad (3)$$

with  $\text{bonds}$  running over all the bonds on the lattice;  $\text{triangles}$  running over all the triangles, up- and down-triangles, on the lattice, while  $\langle 123 \rangle \in P$  are the sites on the triangles labeled counterclockwise;  $\text{rhombi}$  running over all the rhombi and  $\langle 1234 \rangle$  are the sites on a rhombus labeled counterclockwise.  $P_{12}$  is the nearest-neighbor two-site exchange operator,  $P_{123}$  is the three-site spin ring exchange operator, and  $P_{1234}$  is the four-site spin ring exchange operator, Fig. 1. The couplings  $J$ ,  $K_3$ , and  $K_4$  can be obtained from perturbative analysis of SU(3) Hubbard model at  $1/3$  filling and the leading-order terms are

$$J = \frac{2t^2}{U}, \quad (4)$$

$$K_3 = \frac{6t^3}{U^2}, \quad (5)$$

$$K_4 = \frac{20t^4}{U^3}. \quad (6)$$

Without the ring exchange terms, previous studies of the site-factorized ansatz on the triangular lattice predicted a three-sublattice ordered state [18–20] which was recently confirmed by Density Matrix Renormalization Group (DMRG) and infinite Projected Entangled-Pair States (iPEPS) analysis [15].

Recently, Ref. 21 did variational studies on the SU(3) model with three-site ring exchange, and they found the ferromagnetic state and the three-sublattice ordered state in the regime of ferromagnetic three-site ring exchanges. On the anti-ferromagnetic side of the three-site ring exchanges, they found an interesting  $d_x + id_y$  spin liquid state with a gapless parton Fermi surface.

However, the situation is not clear while both the three-site and four-site ring exchange terms are included. Here in this work, we will focus on the regime where the three-site ring exchange is ferromagnetic and the four-site ring exchange is anti-ferromagnetic, motivated by the perturbative studies of SU(3) Hubbard model. In order to study the ordered phases, below in Sec. II A, we first present our studies of ordered phases using the site-factorized states. Later in Sec. II B we will present our studies using the slave-fermion trial states.

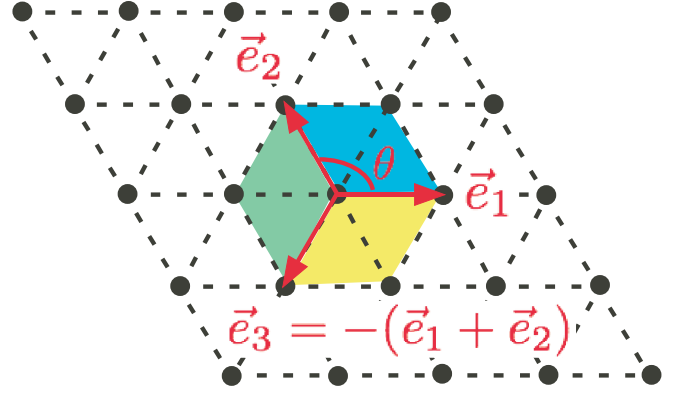


FIG. 1. The triangular lattice showing the vectors  $\vec{e}_{\nu=1,2,3}$  used in the text. The shaded region represents a single rhombi and we label each site counterclockwise from 1 to 4. The angle  $\theta$  between each vector  $\vec{e}$  is  $2\pi/3$ .

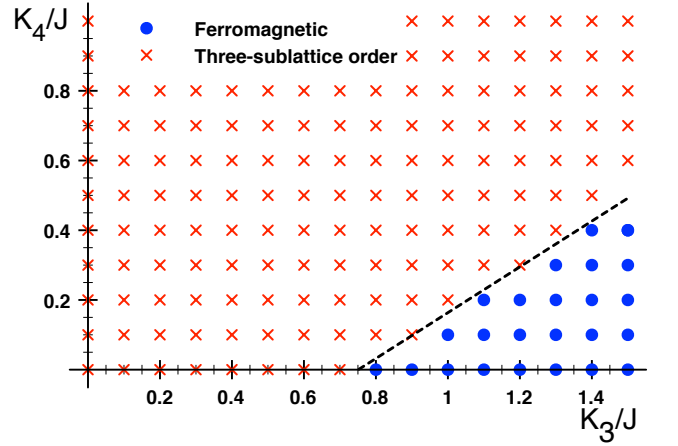


FIG. 2. The phase diagram using the site-factorized states. The red crosses represent the three-sublattice ordered states with each on-site vector, Eq. (7), mutually orthogonal to each other and the closed blue circles represent the ferromagnetic state. The dashed line is the tentative boundary between the two phases. The boundary between the ferromagnetic state and the three-sublattice ordered state can be determined analytically (see text) and consistent with the numerical studies. We note that this model contains a four-sublattice ordered state for strong four-site ring exchange, roughly when  $K_4/J > 1.4$ . In such state, the numerical site-factorized states indeed show a four-sublattice periodicity. However, the four-sublattice ordered state is hard to be characterized analytically.

### A. Site-factorized state studies

In this subsection, we consider the site-factorized state [18] defined as

$$|s\rangle = \prod_j |\mathcal{X}_j\rangle, \quad (7)$$

with

$$|\mathcal{X}_j\rangle \equiv a_j|x\rangle_j + b_j|y\rangle_j + c_j|z\rangle_j, \quad (8)$$

where we fix the overall phase by setting the phase of  $a_j$  to be zero such that  $a_j \in \mathbb{R}$  and  $b_j, c_j \in \mathbb{Z}$  and  $|a_j|^2 + |b_j|^2 + |c_j|^2 = 1$ .

We numerically calculate the site-factorized ansatz state energy,  $E_{sf} = \langle s | H_{SU(3)} | s \rangle$ , on a  $3 \times 3$ , and a  $6 \times 6$  triangular lattice and determine the optimal state in the parameter regime. The phase diagram is shown in Fig. 2. The red crosses represent the states with three-sublattice order with sublattices labeled as  $A$ ,  $B$ , and  $C$ . The three-sublatticed states are characterized with each on-site vector ( $|\mathcal{X}_{j \in A}\rangle$ ,  $|\mathcal{X}_{j \in B}\rangle$ , and  $|\mathcal{X}_{j \in C}\rangle$ ) mutually orthogonal to each other and the closed blue circles represent the ferromagnetic state. We note that this model shows four-sublattice ordered state with strong four-site ring exchange, roughly when  $K_4/J > 1.4$ . In the regime, the numerical values of the site-factorized states show a four-sublattice periodicity. However, the four-sublattice ordered state is hard to be characterized analytically.[22, 23]

The boundary between the three-sublattice order and the ferromagnetic phase can be understood analytically. The three-sublattice state is a state with each on-site vector mutually orthogonal to each other. The state vector for the three-sublattice state has the form  $|\psi\rangle_u = |x\rangle_{j \in A} \otimes |y\rangle_{k \in B} \otimes |z\rangle_{l \in C}$  with  $j, k, l$  around a triangle. Since the state vector at each site is orthogonal to each other, the energy is  $\langle H_{SU(3)} \rangle_{3-sub} = 0$ . On the other hand, the state vectors of a ferromagnetic phase are aligned with each other, say  $|z\rangle$  for all sites. The energy in the ferromagnetic phase is  $\langle H_{SU(3)} \rangle_{FM} = 3J - 4K_3 + 6K_4$ . The boundary between these two phases can be determined analytically from the condition  $3J - 4K_3 + 6K_4 = 0$ . For  $K_4 = 0$ , the transition point is at  $3/4$ , which is consistent with our numerical studies.

## B. Slave-fermion trial states and energetics

In this subsection, we follow the approach similar to the one outlined in Ref. [24] for the spin  $S = 1$ . We write the spin operators in terms of three flavors of fermionic spinons,  $f^\alpha$ ,

$$S_j^\alpha = -i \sum_{\beta, \gamma} \epsilon^{\alpha\beta\gamma} f_j^{\beta\dagger} f_j^\gamma, \quad (9)$$

with  $\alpha, \beta, \gamma \in \{x, y, z\}$  and  $j$  is the site label. Rewriting the spin operator in terms of fermionic spinons enlarges the Hilbert space. To recover the physical subspace, a local constraint on the fermions has to be enforced,

$$\sum_{\alpha} f_j^{\alpha\dagger} f_j^\alpha = 1. \quad (10)$$

The exchange operators in terms of fermions are

$$P_{jk} = \sum_{\alpha\beta} f_j^{\alpha\dagger} f_j^\beta f_k^{\beta\dagger} f_k^\alpha, \quad (11)$$

$$P_{jkl} = \sum_{\alpha\beta\gamma} f_j^{\alpha\dagger} f_j^\beta f_k^{\beta\dagger} f_k^\gamma f_l^{\gamma\dagger} f_l^\alpha, \quad (12)$$

$$P_{jklm} = \sum_{\alpha\beta\gamma\eta} f_j^{\alpha\dagger} f_j^\beta f_k^{\beta\dagger} f_k^\gamma f_l^{\gamma\dagger} f_l^\eta f_m^{\eta\dagger} f_m^\alpha, \quad (13)$$

where  $\alpha, \beta, \gamma, \eta = x, y, z$ .

The Hamiltonian, Eq. (3), can be re-expressed as

$$\begin{aligned} H_{SU(3)} = & J \sum_{\langle jk \rangle} \sum_{\alpha\beta} f_j^{\alpha\dagger} f_j^\beta f_k^{\beta\dagger} f_k^\alpha - \\ & - K_3 \sum_{\langle jkl \rangle} \sum_{\alpha\beta\gamma} \left[ f_j^{\alpha\dagger} f_j^\beta f_k^{\beta\dagger} f_k^\gamma f_l^{\gamma\dagger} f_l^\alpha + \text{H.c.} \right] + \\ & + K_4 \sum_{\langle jklm \rangle} \sum_{\alpha\beta\gamma\eta} \left[ f_j^{\alpha\dagger} f_j^\beta f_k^{\beta\dagger} f_k^\gamma f_l^{\gamma\dagger} f_l^\eta f_m^{\eta\dagger} f_m^\alpha + \text{H.c.} \right] \end{aligned} \quad (14)$$

Below, we will calculate the trial energies using the slave fermion trial states. We start from the case without considering pairing instability. We find that the the main competing states are what we call the “trimer” state, the uniform  $\pi$ -flux spin liquid state, and the zero-flux spin liquid state. Later, focusing on the regime in which spin liquid states are the optimal slave-fermion states, we consider the possible pairing instabilities. We find that there is a possible pairing instability of the zero-flux spin liquid state toward a  $f$ -wave (nodal) spin liquid state and a pairing instability of the  $\pi$ -flux spin liquid state toward an exotic  $s$ -wave spin liquid state with two flavors of fermions paired up while one flavor of fermions remains gapless.

### 1. Without pairing instability

In this section, we focus on the non-magnetic trial states. When we perform numerical calculations, we relax the constraint of the fermion number for each flavor to be

$$\langle f_j^{\alpha\dagger} f_j^\alpha \rangle_{\text{trial}} = \frac{1}{3}. \quad (15)$$

A convenient formulation of the mean field is to consider a general  $SU(3)$ -rotation invariant trial Hamiltonian

$$\begin{aligned} H_{\text{trial}} = & - \sum_{\langle jk \rangle} \sum_{\alpha} \left[ t_{jk} e^{-i\theta_{jk}} f_j^{\alpha\dagger} f_k^\alpha + \text{H.c.} \right] - \\ & - \sum_j \sum_{\alpha} \mu_j f_j^{\alpha\dagger} f_j^\alpha, \end{aligned} \quad (16)$$

with  $t_{jk}$  being the hopping amplitude,  $\theta_{jk}$  being the phase of the hopping  $t_{jk}$  in different mean-field ansatz states, and  $\mu_j$  being the chemical potential which can be used to satisfy the constraint, Eq. (15). With the trial Hamiltonian above, we can find the ground state and use it as a trial wave function for the Hamiltonian  $H_{SU(3)}$ , Eq. (3). After performing “complete” Wick contractions and ignoring the constant pure density terms, the trial energy can be expressed as

$$\begin{aligned}
E_{MF} = & -J \sum_{\text{dimer}} \left| \sum_{\alpha} \chi_{12}^{\alpha} \right|^2 - \\
& -K_3 \sum_{\text{triangle}} \left\{ \left[ \sum_{\alpha} \chi_{12}^{\alpha} \chi_{23}^{\alpha} \chi_{31}^{\alpha} - \sum_{\alpha\beta} \left( n_1^{\alpha} \chi_{23}^{\alpha} \chi_{32}^{\beta} + n_2^{\alpha} \chi_{31}^{\alpha} \chi_{13}^{\beta} + n_3^{\alpha} \chi_{12}^{\alpha} \chi_{21}^{\beta} \right) + \sum_{\alpha\beta\gamma} \chi_{13}^{\alpha} \chi_{32}^{\beta} \chi_{21}^{\gamma} \right] + \text{H.c.} \right\} + \\
& +K_4 \sum_{\text{tetrahedron}} \left\{ \left[ \sum_{\alpha} \left( n_2^{\alpha} \chi_{13}^{\alpha} \chi_{34}^{\alpha} \chi_{41}^{\alpha} + n_4^{\alpha} \chi_{12}^{\alpha} \chi_{23}^{\alpha} \chi_{31}^{\alpha} \right) - \right. \right. \\
& \quad \left. - \sum_{\alpha\beta} \left( n_1^{\alpha} n_2^{\alpha} \chi_{34}^{\alpha} \chi_{43}^{\beta} + n_1^{\alpha} n_4^{\alpha} \chi_{23}^{\alpha} \chi_{32}^{\beta} + n_3^{\alpha} n_4^{\alpha} \chi_{12}^{\alpha} \chi_{21}^{\beta} + n_2^{\alpha} n_3^{\alpha} \chi_{41}^{\alpha} \chi_{14}^{\beta} + n_2^{\alpha} \chi_{31}^{\alpha} n_4^{\beta} \chi_{13}^{\beta} + \chi_{12}^{\alpha} \chi_{34}^{\alpha} \chi_{23}^{\beta} \chi_{41}^{\beta} \right) \right. \\
& \quad \left. + \sum_{\alpha\beta\gamma} \left( \chi_{12}^{\alpha} \chi_{34}^{\alpha} \chi_{21}^{\beta} \chi_{43}^{\gamma} + \chi_{23}^{\alpha} \chi_{41}^{\alpha} \chi_{32}^{\beta} \chi_{14}^{\gamma} + n_2^{\alpha} \chi_{31}^{\alpha} \chi_{14}^{\beta} \chi_{43}^{\gamma} + n_4^{\alpha} \chi_{13}^{\alpha} \chi_{21}^{\beta} \chi_{32}^{\gamma} \right) - \right. \\
& \quad \left. - \sum_{\alpha\beta\gamma\eta} \chi_{14}^{\alpha} \chi_{43}^{\beta} \chi_{32}^{\gamma} \chi_{21}^{\eta} \right] + \text{H.c.} \left. \right\}. \tag{17}
\end{aligned}$$

Above we defined  $(\chi_{jk}^{\alpha})^* \equiv \langle f_j^{\alpha\dagger} f_k^{\alpha} \rangle_{\text{trial}}$ .

The slave-fermion trial states which conserve the translational symmetry we consider in this work are the uniform zero-flux state and uniform  $\pi$ -flux state. The fermions in both of these trial states hop isotropically on the lattice,  $t_{jk} \simeq t$ , and therefore the expectation values of  $\chi_{jk}$  are expected to be isotropic,  $\chi_{jk}^{\alpha} \simeq \chi^{\alpha} = \text{const.}$  Below we list the numerical values of the energy per site in the two states

$$E_{\phi=0}^{MF} = -0.7672J + 0.4482K_3 - 0.4521K_4, \tag{18}$$

$$E_{\phi=\pi}^{MF} = -0.4395J + 0.8352K_3 - 0.7949K_4. \tag{19}$$

We can observe that the optimal translationally invariant slave-fermion state favors  $\phi = 0$  state when  $K_3 > 0$  and  $\phi = \pi$  state when  $K_3 < 0$ . The distinguishability between these two uniform-flux spin liquid states can be related to the origin of the  $K_3$  which arises from the third-order perturbation of the SU(3)Hubbard model at 1/3 filling. However,  $K_4$  does not distinguish these two uniform-flux (U(1)) spin liquid states from this perspective.

Besides the translationally invariant state, we also consider what we call the “trimer” state. Fig. 3 shows one example of the configuration of such a state in which the non-zero  $t_{jk}$  form non-overlapping trimer covering of the lattice. These states break translational invariance, and any trimer covering produces such a state. Such states can have lower Heisenberg exchange energy. The occupied bonds attain the maximal expectation value which is found analytically  $|\chi_{jk}^{\alpha}|_{\text{max}} = n_j^{\alpha} = 1/3$ . Their contribution can be sufficient to produce the lowest total energy and such states are expected to be the lowest-energy states with  $K_3 = 0$  and  $K_4 = 0$ .

$$E_{\text{trimer}}^{MF} = -J + 0.5926K_3 - 0.3704K_4. \tag{20}$$

The energies of different slave-fermion trial states are functions of  $K_3/J$  and  $K_4/J$  and it is expected that different optimal trial state is realized in different parameter regime. In order to clearly show the cross between the energies of different

mean-field ansatz states as functions of  $K_3/J$  and  $K_4/J$ , we plot Eqs. (18)-(20) with  $J \equiv 1$  in the limit of either  $K_3 = 0$  or  $K_4 = 0$ .

Figure 4 shows the energies of different mean-field states as a function of  $K_3/J$  with  $K_4 = 0$  and as a function of  $K_4/J$  with  $K_3 = 0$ . For the former, Fig. 4(a) clearly shows that at  $K_3, K_4 = 0$  the trimer state is the lowest energy state followed by the uniform zero-flux state and  $\pi$ -flux state. When  $K_3$  is gradually increased, the energy line of the zero-flux state crosses that of the trimer state and the zero-flux state becomes the lowest energy state at  $K_3/J \sim 1.61$ . On the other hand, for the latter, Fig. 4(b) shows that the energy line of  $\pi$ -flux state first crosses that of the zero-flux state at  $K_4 \simeq 0.96$  and then crosses that of trimer state. The zero-flux state becomes the lowest energy state at  $K_4 \simeq 1.32$ . For a complete phase diagram, we numerically determine the ground states in the  $K_3 - K_4$  parameter regimes and the result is summarized in the mean-field phase diagram, Fig. 5.

In order to check if the mean-field ansatz states we considered are sufficient to describe the physics in this model, we perform numerically “full optimization” of the mean-field energy, Eq. (17), on a triangular lattice with  $100 \times 100$  3-site unit cells, by treating  $\chi_{jk}$ -s and  $\theta_{jk}$ -s as varying variables. In the numerical optimization, there are totally 18 variables, 9  $\chi_{jk}$  and 9  $\theta_{jk}$ , and we take  $t_{jk} = 1$ ,  $\mu_j^{\alpha} = \mu$ . Numerics suggest that the above trial states are the three optimal states.

Before leaving this section, we want to remark that the trimer state is a singlet state around a triangular plaquette, and we can write down the exact singlet wave function in a closed form as

$$|\psi_{\text{trimer}}\rangle = \sum_{\alpha,\beta,\gamma} \frac{\epsilon^{\alpha\beta\gamma}}{\sqrt{6}} |\alpha, \beta, \gamma\rangle, \tag{21}$$

with  $\alpha = x, y, z$ . With the trimer wave function, we can calculate the energy per site

$$\mathcal{E}_{\psi_{\text{trimer}}} = -\frac{1}{3}J - \frac{4}{27}K_3 + \frac{2}{9}K_4. \tag{22}$$



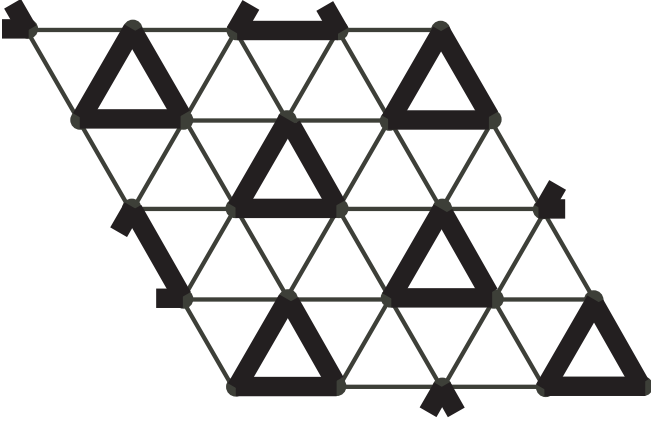


FIG. 3. Illustration of the trimer state. In slave fermion picture, the fermionic spinons only hop around each triangular plaquette and we can focus on each triangle separately.

For  $K_3 = 0$  and  $K_4 = 0$ , the exact trimer state energy is very close to the variational energy of U(1) spin liquid which is  $-0.34J$ [21], but much higher than the three-sublattice order state energy obtained by DMRG which is roughly  $-0.678J$ . [15] However, such a plaquette state can be stabilized with finite  $K_3$  before reaching the ferromagnetic state. To see this, we can compare the energy of the ferromagnetic state as shown analytically in the end of Sec. II A with that of the exact trimer state energy. Knowing the energy of the ferromagnetic state,  $E_{FM} = 3J - 4K_3 + 6K_4$ , we can see that the trimer state indeed has the lower energy than that of the ferromagnetic state when  $K_3/J < \frac{45}{52} + \frac{3}{2}K_4 \simeq 0.86 + 1.5K_4$ .

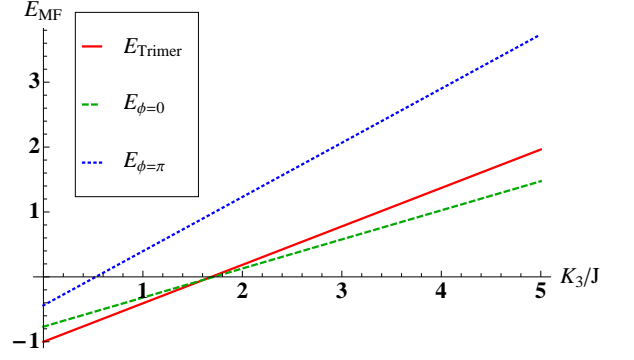
## 2. With pairing instability

So far, we have ignored the possible pairing instabilities in the Fermi surface spin liquid states discussed above. Here we want to address this issue. We now know that besides the trimer state, there are actually two spin liquid states—zero-flux spin liquid state and  $\pi$ -flux spin liquid state. Both of these spin liquid states are gapless and contain a single or multiple parton Fermi surfaces. Focusing on these regimes, we take the pairing mechanism into consideration and the trial Hamiltonian becomes

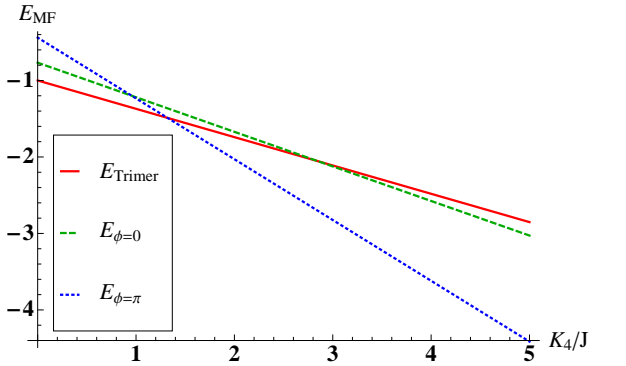
$$H_{trial} = - \sum_{\langle jk \rangle} \sum_{\alpha, \beta} \left[ \left( t_{jk}^{\phi} \delta^{\alpha\beta} f_j^{\alpha\dagger} f_k^{\beta} + \Delta_{jk}^{\alpha\beta} f_j^{\alpha\dagger} f_k^{\beta\dagger} \right) + \text{H.c.} \right] - \sum_j \sum_{\alpha} \mu_j f_j^{\alpha\dagger} f_k^{\alpha}, \quad (23)$$

with the constraint,  $n_j^{\alpha} = \langle f_j^{\alpha\dagger} f_j^{\alpha} \rangle = 1/3$  and  $t_{jk}^{\phi} = \pm t_{jk}$  for flux  $\phi = 0/\pi$ . For clarity, from now on we will replace the bond labeling  $\langle jk \rangle$  by  $(\mathbf{r}, \mathbf{r} + \vec{e}_{\nu})$ , with  $\mathbf{r}$  running over all lattice sites and  $\vec{e}_{\nu=1,2,3}$  are shown in Fig. 1. We abbreviated the sum over all  $\vec{e}_{\nu=1,2,3}$  as  $\vec{e}$ .

In these regimes, the optimal state are uniform flux states which suggests uniform trial hopping amplitude  $t_{jk} \simeq t \equiv 1$



(a) Energies of different trial states energies as a function of  $K_3$  while  $K_4 = 0$



(b) Energies of different trial states as a function of  $K_4$  while  $K_3 = 0$

FIG. 4. (a) Illustration of energies of different slave-fermion trial states as a function of  $K_3$  with  $K_4 = 0$  (b) Illustration of energies of different slave-fermion trial states as a function of  $K_4$  with  $K_3 = 0$ . When  $K_3 = 0$  and  $K_4 = 0$ , the optimal state is the trimer state followed by the zero-flux spin liquid state and the  $\pi$ -flux spin liquid state. When  $K_3$  increases while  $K_4 = 0$ , the zero-flux spin liquid state becomes the lowest-energy state ( $K_3 > 1.61$ ,  $K_4 = 0$ ) as shown in (a). On the other hand, when  $K_4$  increases while  $K_3 = 0$ , the energy line of  $\pi$ -flux spin liquid state first crosses the energy line of the zero-flux spin liquid at ( $K_3 = 0$ ,  $K_4 \simeq 0.96$ ) and then crosses the energy line of trimer state to become the lowest energy state at ( $K_3 = 0$ ,  $K_4 \simeq 1.32$ ). For general cases, the complete mean-field phase diagram is shown in Fig. 5

and the uniform expectation values of hopping functions,  $\langle f^{\alpha\dagger}(\mathbf{r}) f^{\beta}(\mathbf{r} + \vec{e}_{\nu}) \rangle = \delta^{\alpha\beta} \chi^{\alpha*}(\vec{e}_{\nu})$ . Furthermore, in these regimes, the hopping functions,  $\chi^{\alpha}(\vec{e}_{\nu})$ , should be real and are numerically confirmed. Below, we consider two pairing cases: Case (1) corresponds to pairing within the same flavor of fermions. This requires the orbital angular momentum quantum number to be  $l = 1, 3, \dots$  corresponding to  $p_x + ip_y$ ,  $f$ -wave, ... pairing states; Case (2) corresponds to BCS-type pairing with different flavor of fermions. This pairing requires  $l = 0, 2, \dots$  corresponding to  $s$ -wave,  $d_x + id_y, \dots$  pairing states.[21, 24] Below, we discuss the mathematical set up for

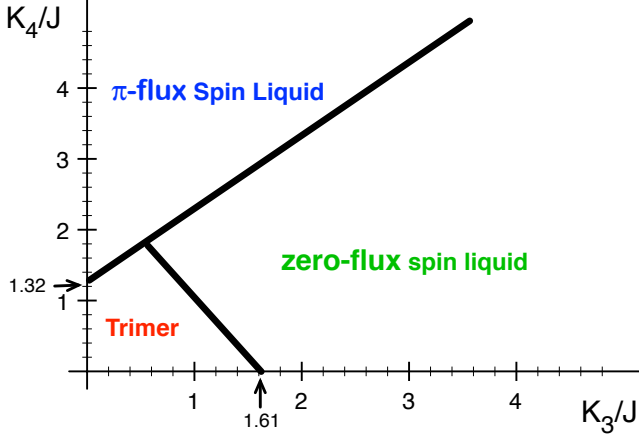


FIG. 5. The phase diagram of the mean-field ansatzes. The lines are the tentative boundaries between different phases. We note that the zero-flux and  $\pi$ -flux spin liquid states are both U(1) Fermi-surface spin liquid states. The difference is that the zero-flux spin liquid state only possesses a single Fermi pocket in the center while the  $\pi$ -flux spin liquid state possesses two Fermi pockets near the hexagonal Brillouin zone. The exact wave function of the trimer state can be written down explicitly, Eq. (21), and we can calculate the corresponding energy exactly.

each case separately.

*Case (1): pairing ansatz with  $\Delta^{\alpha\beta} = \delta^{\alpha\beta} \Delta^\alpha$ .*

The pairing functions we consider are  $\langle f^\alpha(\mathbf{r}) f^\beta(\mathbf{r} + \vec{e}_\nu) \rangle = \delta^{\alpha\beta} \Delta^\alpha(\vec{e}_\nu)$ . By symmetry arguments, the model conserves spatial rotational symmetry and as already explained above, the angular momentum of pairing functions should be odd,  $l = 1, 3, \dots$  corresponding to  $p_x + ip_y$ ,  $f$ -wave pairing,..... The ansatz can be further simplified to be  $\chi^\alpha(\vec{e}_1) = \chi^\alpha(\vec{e}_2) = \chi^\alpha(\vec{e}_3) \equiv \chi^\alpha$ , and  $\Delta^\alpha(\vec{e}_3) = \Delta^\alpha(\vec{e}_2) e^{il \cdot \theta} = \Delta^\alpha(\vec{e}_1) e^{il \cdot 2\theta} \equiv \Delta^\alpha e^{il \cdot 2\theta}$ , where  $\theta$  is  $2\pi/3$  shown in Fig. 1. In addition, because the vectors  $\vec{f} = \{f^x, f^y, f^z\}$  and  $\vec{f}^\dagger = \{f^{x\dagger}, f^{y\dagger}, f^{z\dagger}\}$  transform as a three-dimensional vectors under spin rotation, we expect  $\chi^x = \chi^y = \chi^z \equiv \chi$  and  $\Delta^x = \Delta^y = \Delta^z \equiv \Delta$ . In this pairing scheme, the  $SU(3)$  is broken down to  $SO(3)$ . It is straightforward to diagonalize the mean-field Hamiltonian

$$H_{trial} = \sum_{\alpha} \sum_{\mathbf{k} \in \text{B.Z.}} E_{\alpha}(\mathbf{k}) a^{\alpha\dagger}(\mathbf{k}) a^{\alpha}(\mathbf{k}), \quad (24)$$

where  $a^{\alpha}(\mathbf{k})$  are Bogoliubov quasiparticles satisfying the transformation

$$\begin{pmatrix} f^{\alpha}(\mathbf{k}) \\ f^{\alpha\dagger}(-\mathbf{k}) \end{pmatrix} = \begin{pmatrix} u_{\mathbf{k}}^{\alpha} & -v_{\mathbf{k}}^{\alpha} \\ v_{\mathbf{k}}^{\alpha*} & u_{\mathbf{k}}^{\alpha*} \end{pmatrix} \begin{pmatrix} a^{\alpha}(\mathbf{k}) \\ a^{\alpha\dagger}(\mathbf{k}) \end{pmatrix}, \quad (25)$$

with

$$\begin{aligned} |u_{\mathbf{k}}^{\alpha}|^2 &= \frac{1}{2} \left[ 1 + \frac{\xi_{\alpha}(\mathbf{k})}{E_{\alpha}(\mathbf{k})} \right], \\ |v_{\mathbf{k}}^{\alpha}|^2 &= \frac{1}{2} \left[ 1 - \frac{\xi_{\alpha}(\mathbf{k})}{E_{\alpha}(\mathbf{k})} \right]. \end{aligned} \quad (26)$$

The ground state can be written as

$$|GS\rangle = \prod_{\alpha=x,y,z} \prod_{\mathbf{k}} [u_{\mathbf{k}}^{\alpha} + v_{\mathbf{k}}^{\alpha} f^{\alpha\dagger}(\mathbf{k}) f^{\alpha\dagger}(-\mathbf{k})] |vac\rangle, \quad (27)$$

where we define

$$\xi_{\alpha}(\mathbf{k}) \equiv - \sum_{\vec{e}} 2 \cos(\mathbf{k} \cdot \vec{e}) - \mu, \quad (28)$$

$$\tilde{\Delta}_{\alpha}(\mathbf{k}) \equiv \sum_{\vec{e}} i \Delta \sin(\mathbf{k} \cdot \vec{e}), \quad (29)$$

$$E_{\alpha}(\mathbf{k}) = \sqrt{(\xi_{\alpha}(\mathbf{k})/2)^2 + |\tilde{\Delta}_{\alpha}(\mathbf{k})|^2}. \quad (30)$$

We can see there are three degenerate bands in this case.

*Case (2): pairing ansatz with  $\Delta^{\alpha\alpha} = 0$ ,  $\Delta^{\alpha\beta}|_{\alpha \neq \beta} \neq 0$ .*

We consider the pairing function of the form,  $\langle f^{\alpha}(\mathbf{r}) f^{\beta}(\mathbf{r} + \vec{e}_{\nu}) \rangle_{\alpha \neq \beta} = \Delta^{\alpha\beta}(\vec{e}_{\nu})$ . It seems there are three pairing functions we need to consider,  $\Delta^{xy}$ ,  $\Delta^{yz}$ , and  $\Delta^{zx}$ , but in this  $SU(3)$  symmetric model, we can perform a global gauge transformation to make  $\Delta^{yz}$ ,  $\Delta^{zx} = 0$  as long as the length of the vector formed by  $\Delta$ s is conserved,  $|\Delta^{xy}|^2 + |\Delta^{yz}|^2 + |\Delta^{zx}|^2 = \Delta^2 = \text{constant}$ . [1, 25–29] If this pairing state is energetically favored, there is always one gapless fermion left in this  $SU(3)$  system which we choose to be  $f^z$  in this paper. From now on, we will set  $\Delta^{yz} = \Delta^{zx} = 0$ , while  $\Delta^{xy} = \sqrt{3}\Delta$ . In this gauge choice, the symmetry breaking process is more apparent. The symmetry breaking is  $SU(3) \rightarrow SU(2) \otimes U(1)$ . The  $SU(2)$  symmetry is generated by the pseudo-spin doublet  $f^x$  and  $f^y$  and the  $U(1)$  is generated by the gapless  $f^z$  fermion. After Bogoliubov transformation, the ground state is

$$|GS\rangle = \prod_{\mathbf{k}} [u_{\mathbf{k}}^{xy} + v_{\mathbf{k}}^{xy} f^{x\dagger}(\mathbf{k}) f^{y\dagger}(-\mathbf{k})] |vac\rangle \otimes \quad (31)$$

$$\otimes \sum_{\xi_{\mathbf{k}}^z < 0} f^{z\dagger}(\mathbf{k}) |vac\rangle, \quad (32)$$

where the second part, Eq. (32), is the wave function of the free  $f^z$  fermion, and  $u_{\mathbf{k}}^{xy}$  and  $v_{\mathbf{k}}^{xy}$  have the same expression as in Eq. (26) with  $\xi^x(\mathbf{k}) = \xi^y(\mathbf{k}) = \xi^z(\mathbf{k}) \equiv \xi(\mathbf{k})$  the same to Eq. (28) and

$$\tilde{\Delta}^{xy}(\mathbf{k}) \equiv \sum_{\vec{e}} \sqrt{3}\Delta \cos(\mathbf{k} \cdot \vec{e}), \quad (33)$$

$$E^{xy}(\mathbf{k}) = \sqrt{(\xi(\mathbf{k}))^2 + |\tilde{\Delta}^{xy}(\mathbf{k})|^2}. \quad (34)$$

We can see in the  $SU(3)$ -symmetric point, the energy bands always show one gapless branch corresponding to one flavor of gapless fermions.

With the two pairing ansatzes above, we focus on the regimes where the zero-flux spin liquid state and the  $\pi$ -flux spin liquid state are realized as shown in Fig. 5. We again perform full Wick contractions and ignore the pure constant density terms. The trial energy expression after Wick contractions is too complex to write out explicitly. We test all different pairing ansatzes above and numerically calculate the trial

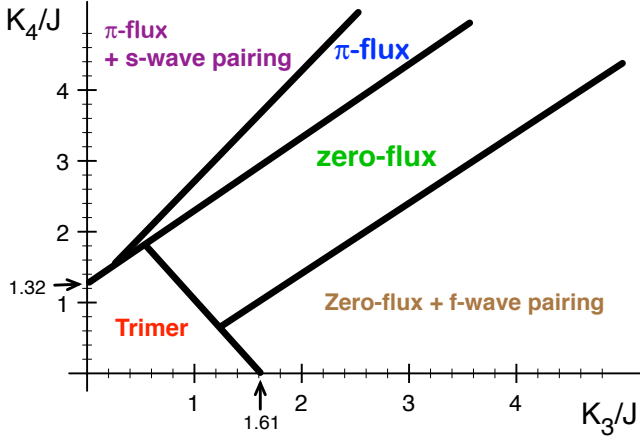


FIG. 6. The mean-field phase diagram with pairing instability. The lines are the tentative boundaries between different states. We note that the line separating the  $\pi$ -flux and zero-flux spin liquid states and the line between zero-flux and trimer state are the same as shown in Fig. 5. Compared with Fig. 5, the phase diagram shows that the zero-flux spin liquid state has a possible pairing instability toward a  $f$ -wave gapless (nodal) spin liquid state, and the  $\pi$ -flux spin liquid state has a possible pairing instability toward a  $s$ -wave spin liquid state with two flavors of fermions paired up while one flavor of fermions remain gapless.

energies with the optimal pairing functions  $\Delta$  in the uniform-flux spin liquids regime on the triangular lattice with  $300 \times 300$  sites.

The result is summarized in Fig. 6. We find that roughly in the regime where the ferromagnetic three-site ring exchanges slightly dominant, the zero-flux spin liquid state (gapless spin liquid with parton Fermi surface) has the pairing instability toward a  $f$ -wave gapless (nodal) spin liquid. When the four-site ring exchange  $K_4$  is strong enough, the pairing instability can be suppressed and the optimal state is the zero-flux spin liquid with Fermi surfaces. However, when we keep increasing  $K_4$ , the optimal state becomes the uniform  $\pi$ -flux spin liquid state. Interestingly, in the  $\pi$ -flux spin liquid state, roughly when the four-site ring exchanges dominant, such a  $\pi$ -flux spin liquid state has the pairing instability toward an exotic  $s$ -wave spin liquid state with  $f^x$  pair with  $f^y$ , which forms a pseudo-spin singlet, while  $f^z$  remains gapless. We note that we numerically find no pairing instability of the uniform spin liquid states toward  $p_x + ip_y$  spin liquid states or  $d_x + id_y$  spin liquid states in the focusing regime where  $K_3, K_4 > 0$ .

### III. DISCUSSION

We study the SU(3) ring-exchange model with “ferromagnetic” three site ring exchanges and “anti-ferromagnetic” four-site ring exchanges. We first use the site-factorized ansatz to study the model and find the three-sublattice ordered states, ferromagnetic states in a large regime of  $K_3 - K_4$  parameter regime.

In the slave-fermion trial states studies, we find the main

competing states are the trimer state, uniform  $\pi$ -flux spin liquid state and the zero-flux spin liquid. The trimer state is strongly suppressed by increasing the strength of the ring exchanges. We also find that the zero-flux state has a possible pairing instability toward a  $f$ -wave gapless (nodal) spin liquid and the  $\pi$ -flux spin liquid state has a pairing instability toward an exotic  $s$ -wave spin liquid state with  $f^x$  pairing with  $f^y$  fermions while  $f^z$  fermions remain gapless.

These gapless spin liquid states have different properties and can be distinguished, at least in the mean-field picture. For clarity, below we will consider specifically the spin correlations,  $\langle \vec{S}_j \cdot \vec{S}_k \rangle_{conn}$  and the (nematic) correlations of diagonal elements of traceless quadrupolar tensor,  $\langle Q_j^{\alpha\alpha} Q_k^{\alpha\alpha} \rangle_{conn}$  with  $Q_j^{\alpha\beta} = (S_j^\alpha S_j^\beta + S_j^\beta S_j^\alpha)/2 - \delta^{\alpha\beta}/3$ . Above we defined the connected correlations  $\langle \mathcal{O}_j^\dagger \mathcal{O}_k \rangle_{conn} \equiv \langle \mathcal{O}_j \mathcal{O}_k \rangle - \langle \mathcal{O}_j^\dagger \rangle \langle \mathcal{O}_k \rangle$ . Before jumping into the discussions of the properties of different spin liquid states, we first note that the correlation functions of the diagonal elements of the quadrupolar tensor can be expressed as

$$\langle Q_j^{\alpha\alpha} Q_k^{\alpha\alpha} \rangle_{conn} = \frac{4}{9} - \left| \langle f_j^{\alpha\dagger} f_k^\alpha \rangle \right|^2, \quad (35)$$

where above we used the identity,  $Q_j^{\alpha\beta} = \delta^{\alpha\beta} - f_j^{\alpha\dagger} f_j^\alpha$  with the constraint  $\sum_\alpha f_j^{\alpha\dagger} f_j^\alpha = 1$ . [21] We can see the first constant is universal for different spin liquid states, but the second contribution is qualitatively different in different spin liquid states can be used for characterizing different spin liquid state. For simplicity of discussion, we define  $\langle Q_j^{\alpha\alpha} Q_k^{\alpha\alpha} \rangle_-$ . We will also discuss the thermal properties of each spin liquid state.

*Properties of uniform-flux (U(1)) spin liquid states:* The uniform zero-flux and  $\pi$ -flux spin liquid states are both U(1) (Fermi-surface) spin liquid states. The zero-flux spin liquid possesses a single parton Fermi pocket in the center and the  $\pi$ -flux spin liquid possesses two parton Fermi pockets near the hexagonal Brillouin zone. In these two different U(1) spin liquid states,

$$\begin{aligned} \langle \vec{S}_j \cdot \vec{S}_k \rangle_{conn}^{mf} &\sim \langle Q_j^{\alpha\alpha} Q_k^{\alpha\alpha} \rangle_{conn}^{mf} \sim \\ &\sim \frac{1 + \cos[(\mathbf{k}_{FR} - \mathbf{k}_{FL}) \cdot (\mathbf{r}_k - \mathbf{r}_j)]}{|\mathbf{r}_k - \mathbf{r}_j|^3}, \end{aligned} \quad (36)$$

where the  $\mathbf{k}_{FR/L}$  represent the momenta of the right patch and the left patch of the Fermi surface for an observable direction. Since the two Fermi surface spin liquid states have different geometric information of Fermi surfaces, the corresponding wave vectors are quantitatively different and can be detected by studying the corresponding spin structure factors. Since the uniform-flux spin liquid states have gapless parton Fermi surface(s), we expect to see linear-temperature dependent specific heat ( $C_v \propto T$ ) and thermal conductivity ( $\kappa \propto T$ ).

*Properties of f-wave gapless (nodal) spin liquid state:* This spin liquid state possesses gapless nodal points. Interestingly, even though the pairing break the original SU(3) symmetry,

the  $SO(3)$  rotational symmetry related to the spin rotation is still preserved (because of the fact that  $\vec{f}$  and  $\vec{f}^\dagger$  with  $\vec{f} \equiv (f^x, f^y, f^z)$  transform as three-dimensional vectors). As far as the low-energy physics is concerned, this spin liquid state possesses

$$\langle \vec{S}_j \cdot \vec{S}_k \rangle_{conn}^{mf} \sim \langle Q_j^{\alpha\alpha} Q_k^{\alpha\alpha} \rangle_-^{mf} \sim \frac{1 + \cos[\mathbf{k}_c \cdot (\mathbf{r}_k - \mathbf{r}_j)]}{|\mathbf{r}_k - \mathbf{r}_j|^4}, \quad (37)$$

with  $\mathbf{k}_c$  being the vectors connecting different Dirac points and we ignore all the pre-factors of each term in the above equation. Since this spin liquid state contains gapless nodal points, it should possess square-temperature specific heat ( $C_v \propto T^2$ ).

*Properties of the exotic s-wave spin liquid state:* This spin liquid state possesses *short-ranged* spin correlations due to the superconducting gap in the  $x$ - $y$  channel. In order to detect the gaplessness of such a spin liquid state, we can measure the correlation functions of different diagonal elements of the quadrupolar tensor. For example, the  $Q^{zz}$  correlation will show the power-law behavior

$$\langle Q_j^{zz} Q_k^{zz} \rangle_-^{mf} \sim \frac{1 + \cos[(\mathbf{k}_{FR}^z - \mathbf{k}_{FL}^z) \cdot (\mathbf{r}_k - \mathbf{r}_j)]}{|\mathbf{r}_k - \mathbf{r}_j|^3}, \quad (38)$$

with  $\mathbf{k}_{FR/L}^z$  being the momenta of the right patch and the left patch of the  $f^z$  Fermi surface. But the correlations related to  $Q^{xx}$  and  $Q^{yy}$  exponentially decay. As for the thermal properties, we expect to see  $C_v \propto T$  and  $\kappa \propto T$  due to the gapless  $f^z$  parton Fermi surface.

We remark that in the slave-fermion trial states studies, we only focus on the non-magnetic trial states and fix the number density of each flavor to be equal,  $n_j^\alpha = \langle f_j^{\alpha\dagger} f_j^\alpha \rangle = 1/3$ . In principle, we can also consider the magnetic ordered states by making the number density of each flavor per site different as, for example,  $\langle f_j^{z\dagger} f_j^z \rangle = 1$ , and  $\langle f_j^{x\dagger} f_j^x \rangle = 0 = \langle f_j^{y\dagger} f_j^y \rangle$ . After Gutzwiller projection of all the fermionic mean-field states (magnetic ordered states and non-magnetic states) [30], we can compare the energies of different states.

From the perspective of numerics, since there have been DMRG and iPEPS studies on the  $SU(3)$  Heisenberg model of

three-flavor fermions on the triangular lattice which found the three-sublattice ordered state. [15] We suggest possibly the interesting zero-flux spin liquid state be also detected in the DMRG and iPEPS studies on the  $SU(3)$  ring-exchange model.

From the view of cold atom experiments. Recently, the cold atom experiment demonstrated a method to be able to add an artificial tunable gauge potential to the system. [31] With the tunable gauge potential, it may be possible to tune the sign of the three-site ring exchanges from ferromagnetic to anti-ferromagnetic. In that case, for strong four-site ring exchange, the main competing states are still the zero-flux and  $\pi$ -flux spin liquid states, with the trial energies similar to Eqs (18)-(19) with  $K_3 < 0$ . However, for small  $K_4$ , the main competing slave-fermion trial states are the uniform  $\pi/3$ -flux spin liquid state with the trial energy,  $E_{\phi=\pi/3}^{MF} \simeq -0.8992J + 0.8343K_3 + 0.02443K_4$ , and the  $\pi$ -flux spin liquid state. It may be interesting to explore the regime with anti-ferromagnetic three-site ring exchange with  $K_4 \sim 0$  and it may be possible to see a phase transition between these two spin liquid states by manipulating the artificial gauge potential in experiment.

Another interesting theoretical outlook is how the phase diagram, Fig. 6, evolves if we perturb the model away from the  $SU(3)$ -symmetric point. In this way, the model can be connected to other models [21, 24, 32] which can explain the gapless spin-1 spin liquids possibly realized in  $Ba_3NiSb_2O_9$  [33] or other theoretical spin-1 models. [19, 20, 34–36]

## ACKNOWLEDGMENTS

The author would like to thank deeply Olexei I. Motrunich for his suggestions and critically read the initial manuscript. The author thanks Kun Yang, Yuan-Ming Lu, Gang Chen, Maksym Serbyn, Samuel Bieri, and Frederic Mila for helpful discussion. The author is supported by National Science Foundation under Grant No. DMR-1004545 and DMR-0907145. The author also would like to thank KITP where the research is completed and is supported in part by the National Science Foundation under Grant No. NSF PHY11-25915.

- 
- [1] C. Honerkamp and W. Hofstetter, Phys. Rev. Lett. **92**, 170403 (2004).
  - [2] M. A. Cazalilla, A. F. Ho, and M. Ueda, New Journal of Physics **11**, 103033 (2009).
  - [3] T. Fukuhara, S. Sugawa, M. Sugimoto, S. Taie, and Y. Takahashi, Phys. Rev. A **79**, 041604 (2009).
  - [4] S. Taie, Y. Takasu, S. Sugawa, R. Yamazaki, T. Tsujimoto, R. Murakami, and Y. Takahashi, Phys. Rev. Lett. **105**, 190401 (2010).
  - [5] C. Wu, J.-p. Hu, and S.-c. Zhang, Phys. Rev. Lett. **91**, 186402 (2003).
  - [6] A. Gorshkov, M. Hermele, V. Gurarie, C. Xu, P. S. Julienne, J. Ye, P. Zoller, E. Demler, M. D. Lukin, and A. M. Rey, Nature Physics **6**, 289 (2010).
  - [7] M. K. Tey, S. Stellmer, R. Grimm, and F. Schreck, Phys. Rev. A **82**, 011608 (2010).
  - [8] C. Xu, Phys. Rev. B **81**, 144431 (2010).
  - [9] R. Jordens, N. Strohmaier, K. Gunter, H. Moritz, and T. Esslinger, Nature **455**, 204 (2008).
  - [10] U. Schneider, L. Hackermüller, S. Will, T. Best, I. Bloch, T. A. Costi, R. W. Helmes, D. Rasch, and A. Rosch, Science **322**, 1520 (2008).
  - [11] O. I. Motrunich, Phys. Rev. B **72**, 045105 (2005).
  - [12] H.-Y. Yang, A. M. Läuchli, F. Mila, and K. P. Schmidt, Phys. Rev. Lett. **105**, 267204 (2010).
  - [13] M. Hermele and V. Gurarie, Phys. Rev. B **84**, 174441 (2011).
  - [14] Z. Cai, H.-H. Hung, L. Wang, Y. Li, and C. Wu, arXiv:1207.6843 (unpublished).



- [15] B. Bauer, P. Corboz, A. M. Läuchli, L. Messio, K. Penc, M. Troyer, and F. Mila, Phys. Rev. B **85**, 125116 (2012).
- [16] P. A. Lee, N. Nagaosa, and X.-G. Wen, Rev. Mod. Phys. **78**, 17 (2006).
- [17] L. Balents, Nature **464**, 199 (2010).
- [18] A. Läuchli, F. Mila, and K. Penc, Phys. Rev. Lett. **97**, 087205 (2006).
- [19] N. Papanicolaou, Nuclear Physics B **305**, 367 (1988).
- [20] H. Tsunetsugu and M. Arikawa, Journal of the Physical Society of Japan **75**, 083701 (2006).
- [21] S. Bieri, M. Serbyn, T. Senthil, and P. A. Lee, arXiv:1208.3231v1 (unpublished).
- [22] The four-sublattice ordered state can be possibly analyzed numerically by considering the helical states. The helical state can be constructed by first choosing the site-factorized vectors  $\vec{\mathcal{X}}_l$  and  $\vec{\mathcal{X}}_{l+1}$  of two consecutive stripes (in the basis of  $\{|x\rangle, |y\rangle, |z\rangle\}$ ), and we can write the next one as  $\vec{\mathcal{X}}_{l+2} = \cos \theta \vec{\mathcal{X}}_l + \sin \theta \vec{\mathcal{X}}_l^\dagger \times \vec{\mathcal{X}}_{l+1}^\dagger$ .
- [23] T. A. Tóth, A. M. Läuchli, F. Mila, and K. Penc, Phys. Rev. Lett. **105**, 265301 (2010).
- [24] M. Serbyn, T. Senthil, and P. A. Lee, Phys. Rev. B **84**, 180403 (2011).
- [25] C. Honerkamp and W. Hofstetter, Phys. Rev. B **70**, 094521 (2004).
- [26] L. He, M. Jin, and P. Zhuang, Phys. Rev. A **74**, 033604 (2006).
- [27] R. W. Cherng, G. Refael, and E. Demler, Phys. Rev. Lett. **99**, 130406 (2007).
- [28] C. K. Chung and C. K. Law, Phys. Rev. A **82**, 033620 (2010).
- [29] K. M. O'Hara, New Journal of Physics **13**, 065011 (2011).
- [30] X.-G. Wen, Phys. Rev. B **65**, 165113 (2002).
- [31] J. Struck, C. Ölschläger, M. Weinberg, P. Hauke, J. Simonet, A. Eckardt, M. Lewenstein, K. Sengstock, and P. Windpassinger, Phys. Rev. Lett. **108**, 225304 (2012).
- [32] C. Xu, F. Wang, Y. Qi, L. Balents, and M. P. A. Fisher, Phys. Rev. Lett. **108**, 087204 (2012).
- [33] J. G. Cheng, G. Li, L. Balicas, J. S. Zhou, J. B. Goodenough, C. Xu, and H. D. Zhou, Phys. Rev. Lett. **107**, 197204 (2011).
- [34] S. Bhattacharjee, V. B. Shenoy, and T. Senthil, Phys. Rev. B **74**, 092406 (2006).
- [35] Z.-X. Liu, Y. Zhou, and T.-K. Ng, Phys. Rev. B **81**, 224417 (2010).
- [36] T. Grover and T. Senthil, Phys. Rev. Lett. **107**, 077203 (2011).